Shedding Light on the Operation of Polymer Light-Emitting Electrochemical Cells Using Impedance Spectroscopy

*Antoni Munar, Andreas Sandström, Shi Tang, and Ludvig Edman**

A combination of impedance spectroscopy, device characterization, and modeling is used to pinpoint key processes in the operation of polymer light-emitting electrochemical cells (LECs). At low applied voltage, electric double layers with a thickness of ≈2–3 nm are shown to exist at the electrode interfaces. At voltages exceeding the bandgap potential of the conjugated polymer ($V \geq 2.5$ V for superyellow), a light-emitting p–n junction forms in situ, with a steady-state structure that is found to depend strongly on the applied voltage. This is exemplified by that the effective p–n junction thickness (d_{pn}) for a device with an interelectrode gap of 90 nm decreases from ≈23 nm at 2.5 V to ≈6 nm at 3.9 V. The current increases with decreasing d_{pn} in a concerted manner, while the brightness reaches its peak at $V = 3.4$ V when $d_{pn} \approx 10$ nm. The existence of an optimum d_{pn} for high brightness in LECs is attributed to an offset between an increase in the exciton formation rate with decreasing d_{pn}, due to an increasing current, and a simultaneous decrease in the exciton radiative decay rate, when an increasing fraction of excitons diffuses away from the p–n junction into the surrounding non-radiative doping regions.

1. Introduction

The light-emitting electrochemical cell (LEC)[1–13] is an interesting alternative to the more commonplace organic light-emitting diode (OLED)[11,14–20] in that it presents practical advantages, notably the opportunity for use of air-stable materials fit for a low-cost continuous solution-based fabrication,[21–26] as well as unique and stimulating academic challenges.[27–29] The distinguishing feature between the LEC and the OLED is that the former comprises mobile ions intermixed with the emissive organic semiconductor (OSC) in the active layer, which redistribute following the application of a voltage. That this initial ionic redistribution has a profound influence on the subsequent electronic and emissive function of the LEC is firmly established, but the principle mechanism behind the ion-induced improved function has been under intense debate.[1,3,29–35] However, van Reenen and co-workers recently introduced a "unifying model" that apparently resolved this debate by showing that the key opposing models in fact are limiting cases of the same master model.[36] The same authors also provided experimental support for their model via electrostatic profiling data recorded on planar LEC devices with large interelectrode gaps of ≈100 μm.[28,36]

In parallel with these more fundamental studies, the device performance of more practical sandwich-cell LECs with much smaller sub-micrometer-sized interelectrode gaps have been improved in a rather dramatic fashion recently.[37–44] The obvious question that then arises is whether results obtained on planar devices with large-interelectrode gaps[45,46] carry over to sandwich cells with several orders of magnitude smaller gaps. Moreover, it is of interest and importance to attain information that is lacking about the kinetic and structural aspects of the charge carrier distributions in place in recent state-of-the art sandwich-cell LECs, so that the device performance can be further improved via rational and motivated design principles.

In this article, we present results derived from a systematic impedance spectroscopy, optoelectronic characterization, and modeling study on sandwich-cell LECs and OLEDs. We note that key preceding impedance spectroscopy studies on LECs in the scientific literature have utilized different equivalent circuits for their analysis of recorded data,[47–50] and mention that one of our goals with this study is to introduce complete equivalent circuits based on motivated physical insights. We find that the initial process in LECs biased at low voltages is the formation of electric double layers (EDLs) at the electrode interfaces with a thickness of 2–3 nm. These ion-based EDLs assist with the subsequent efficient and balanced injection of electrons/holes into the OSC (here, the conjugated polymer superyellow (SY)) at the cathodic/anodic interface when the applied voltage exceeds the energy-gap potential of the OSC. The injected electrons/holes attract electrostatically compensating counter ions in an in situ electrochemical doping process, with the end result being the formation of a light-emitting p–n junction doping structure in the bulk of the OSC. We find that the effective thickness of the undoped p–n junction under steady-state conditions depends strongly on the applied voltage, as it decreases from ≈23 nm at 2.5 V to ≈6 nm at 3.9 V in 90-nm-thick sandwich cells. The p–n junction resistance and device current increase in a concerted manner with decreasing p–n

Dr. A. Munar, A. Sandström, Dr. S. Tang, Prof. L. Edman
Department of Physics
Umeå University
SE-90187 Umeå, Sweden
E-mail: ludvig.edman@physics.umu.se
Dr. A. Munar
Department of Physics
Universitat Jaume-I
Castelló de la Plana, 12071, Spain

DOI: 10.1002/adfm.201102687

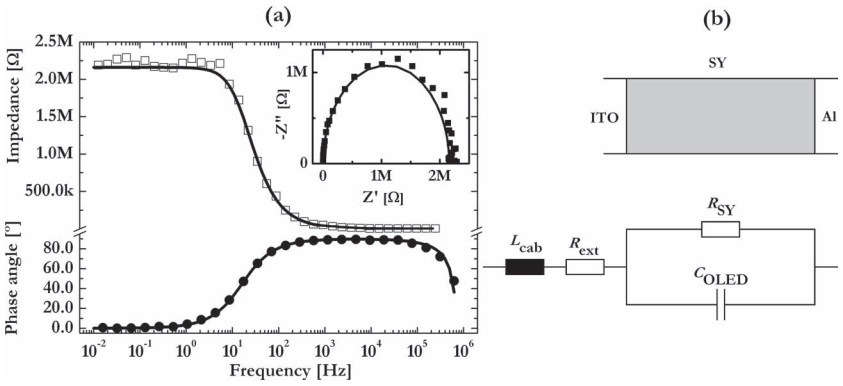

Figure 1. a) The impedance (open squares, top part) and the phase angle (solid circles, bottom part) as a function of frequency for an ion-free ITO/SY/Al OLED operating at V_{DC} = 0 V. The upper right inset presents the corresponding Nyquist plot. The solid lines represent the best fit of the equivalent-circuit parameters to the measured data. b) A schematic picture of the OLED device structure (top) and the employed equivalent circuit (bottom).

junction thickness, while the brightness of the device reaches a maximum at an intermediate thickness of ≈10 nm at 3.4 V. We rationalize this observation with that while a smaller undoped p–n junction thickness invariably is attractive from a conductivity viewpoint, it is negative from an emission-efficiency viewpoint when the precursors of light emission (the excitons) are increasingly able to diffuse out into the exciton-quenching doping regions.

2. Results and Discussion

2.1. Ion-Free OLED Device: Extracting Baseline Data and Building a Model

The impedance spectrum of an indium tin oxide (ITO)/SY/Al device recorded at V_{DC} = 0 V is presented in **Figure 1**a. Note that this device is an OLED, since no mobile ions exist in the active material, which consists solely of the conjugated polymer SY. We choose to begin our investigations with an OLED, since its simple device structure provides a straightforward baseline for the equivalent-circuit development and enables a robust extraction of various device parameters, as detailed below.

Figure 1b presents a schematic of the OLED device structure (top part) and the selected equivalent circuit (bottom part). The latter consists of a parallel circuit, comprising a resistance (R_{SY}), representing the effective resistance of the SY active layer including the injection resistances, and a device capacitance (C_{OLED}), representing the geometric capacitance of the two electrodes contacting the SY film. This parallel circuit is connected in series with a second resistance (R_{ext}), representing all external resistances including those of the ITO and Al electrodes, and an inductance (L_{cab}), representing the inductance of the measurement cables. The latter was measured to be 1.5 μH in a "blank" measurement preceding the device measurements and L_{cab} has accordingly been locked to this value throughout all modeling presented herein.

The fitting of the equivalent circuit to the measured data was executed with a complex non-linear least-squares fitting method,[51] and the resulting parameter data are presented in **Table 1**. The observed good agreement between the experimental data and the modeling results (solid lines) in Figure 1a yields support for that the selected equivalent circuit is an appropriate choice. The external resistance R_{ext} is dominated by the ITO anode, and the output from the modeling, ranging between 20–35 Ω for different devices, is in good agreement with the measured sheet resistance of the employed ITO electrodes.

Table 1. Equivalent circuit data for an OLED operating at V_{DC} = 0 V.

L_{cab} [μH]	R_{ext} [Ω]	R_{SY} [Ω]	C_{OLED} [nF]
1.5	34	2.2×10^6	4.5

The device capacitance C_{OLED} can be used for the calculation of the dielectric constant (ε_r) of the active layer (i.e., SY in the case of the OLED) using the following equation:

$$C = (\varepsilon_r \varepsilon_0 A)/d \quad (1)$$

where ε_0 is the vacuum permittivity, A is electrode interfacial area (= 0.13 cm^2), and d is the thickness of the active layer (= 80 nm for the OLED, as measured using atomic force microscopy). The calculated value for the dielectric constant of SY is ε_r(SY) = 3.1, which is in good agreement with literature data.[52] An effective conductivity for the undoped and ion-free SY film can finally be calculated using the following equation:

$$\sigma = d/(AR) \quad (2)$$

with $R = R_{SY}$. We find that σ(SY, undoped) = 3×10^{-11} S cm^{-1}, and note that such a very low value is reasonable for an undoped conjugated plymer.

2.2. The Electric Double Layer Formation

The formation of EDLs at the two electrode/active material interfaces is the undisputed first step in the operation of an LEC. As (limited unipolar) electronic charge injection into the conjugated polymer can take place at an applied steady-state voltage below the "bandgap potential" of the conjugated ($V_{DC} < E_g/e$, where E_g is the highest occupied molecular orbital (HOMO) - lowest unoccupied molecular orbital (LUMO) gap),[53,54] it is appropriate to probe the EDL formation process at V_{DC} = 0 V. **Figure 2**a presents the impedance spectrum of an ITO/{SY+polyethylene oxide (PEO)+KCF_3SO_3}/Al LEC recorded at V_{DC} = 0 V, and it is clear that the addition of ions into the active layer (top part, Figure 2b) produces a distinctly different impedance response as compared to that of the OLED device presented in Figure 1a).

The equivalent circuit has been expanded with an additional (bottom) path connected in parallel with elements representing

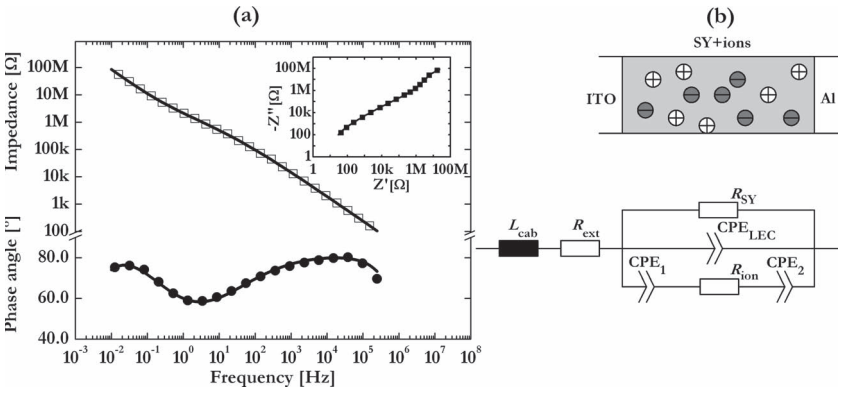

Figure 2. a) The impedance (open squares, top part) and phase angle (solid circles, bottom part) as a function of frequency recorded on an LEC device operating at V_{DC} = 0 V. The inset presents the corresponding Nyquist plot. The solid lines represent the best fit of the equivalent-circuit parameters to the measured data. b) A schematic picture of the LEC device structure (top) and the employed equivalent circuit (bottom).

the resistance of the SY film and the device capacitance (see bottom part, Figure 2b). This new path reflects the existence of ions within the active layer and comprises two constant phase elements (CPEs) and one resistor (R_{ion}), which represent the two EDLs at the electrode/active material interfaces and the bulk ionic resistance of the active layer, respectively. L_{cab} and R_{ext} represent the same as for the OLED device in Figure 1, and the value for R_{ext} is as expected found to be relatively independent on the device type. R_{SY} is observed to be significantly larger for the LEC operating at V_{DC} = 0 V in comparison to the OLED, which can be attributed to the diluting and/or "road blocking" effect of the electrolyte intermixed with SY in the active layer of the LEC device.

It is notable that in order to attain a good fit of the model to the experimental data we found it necessary to include CPEs instead of pure capacitances for the LEC device (see Supporting Information, Section S1).[55] The need for CPE elements is generally attributed to the existence of surface and/or bulk heterogeneities or to continuously distributed time constants for charge-transfer reactions.[56] In the case of our LEC devices under conditions of no charge injection (i.e., at V_{DC} = 0 V), we propose that the origin to the observed CPE behavior is the well-established phase separation between the hydrophobic (and hard) conjugated polymer and the hydrophilic (and soft) electrolyte within the active layer and the concomitant formation of a non-homogenous active layer.

The impedance of a CPE is given by

$$Z_{CPE} = 1/(Q(jw)^n) \quad (3)$$

where ω is the frequency, Q and n ($0 \le n \le 1$) are frequency-independent parameters, and j is the imaginary number. The interpretation of Q depends on n and cannot be directly associated to a meaningful physical value, with the exception that for n = 1 Q is a pure capacitance, and for n = 0, Q is a pure resistor.[56] Nevertheless, it is possible to extract an effective device capacitance (C_{eff}) for other n values, via an approach developed by Hirschorn et al.[56] and Brug et al.,[57] using the following equation:

$$C_{eff} = Q^{1/n} R_i^{(1-n)/n} \quad (4)$$

where R_i represents a series resistance in a "blocking-electrode" scenario (e.g., during the double-layer formation when $R_i = R_{ion}$) and a parallel resistance in a "non-blocking electrode" scenario (e.g., for CPE_{LEC} when $R_i = R_{SY}$). By inserting the parameter values for CPE_{LEC} (**Table 2**), we find that the effective capacitance of the LEC device is C_{LEC} = 29 nF. By then employing Equation (1) and using measured geometric data for the LEC device under study (A = 0.13 cm^2, d = 90 nm), we obtain a value for the dielectric constant of ε_r(LEC) = 22. The much higher dielectric constant for the bulk active layer in the LEC as compared to the OLED (22 vs. 3.1) is consistent with the existence of a high concentration of ions within the active layer of the LEC.

We choose to include two different CPEs for the two EDLs, as an equivalent circuit comprising solely one CPE (or one or two capacitors) for the EDLs failed to accurately model the measured data. One of the CPEs (CPE_2) is found to exhibit a rather low n value, and we suggest that the corresponding EDL is located at the Al cathode interface, as the thermal evaporation of Al onto a phase-separated active layer surface comprising a blend of a soft electrolyte and a hard conjugated polymer should result in a rather inhomogeneous cathodic interface (although the anodic interface also can be expected to be inhomogenous based on the typical uneven surface structure of ITO). In order to facilitate a straightforward structural analysis of the EDL structure in a sandwich-cell LEC, we choose to focus on CPE_1 with an n value of 1, i.e., a purely capacitive element. By approximating the EDL structure with that of a planar capacitor (in agreement with the Helmholtz model) and assuming that the space between the ion-layer in the active material and the ITO electrode surface is filled with an ion-free mixture comprising 67% SY (ε_r = 3.1, see Section 2.1) and 33% PEO (ε_r = 6; see ref. [58]) with an effective ε_r(SY + PEO) of 4, we can use Equation (1) to calculate the thickness of the EDL to 2.7 nm. Such a minute barrier width will allow for facile tunneling injection of electronic charge carriers into the SY conjugated polymer during steady-state operation at $V_{DC} \ge E_g/e$. Moreover, it is plausible that the structure of the EDL is influenced by the applied

Table 2. Equivalent circuit data for an LEC operating at V_{DC} = 0 V.

L_{cab} [μH]	R_{ext} [Ω]	R_{SY} [Ω]	R_{ion} [Ω]	CPE_{LEC}		CPE_1		CPE_2	
				Q [$\times 10^{-7}$]	n	Q [$\times 10^{-7}$]	n	Q [$\times 10^{-7}$]	n
1.5	23	5.0×10^8	$\approx 2 \times 10^3$	0.23	0.91	1.7	1	2.1	0.43

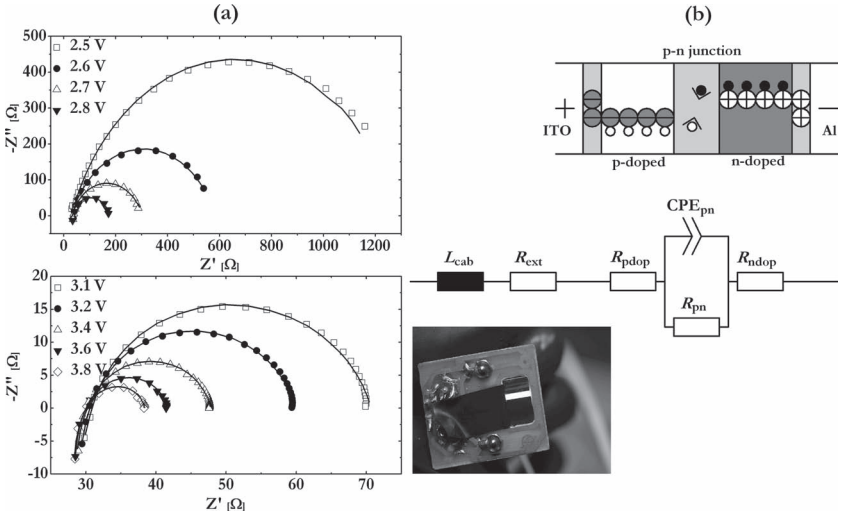

Figure 3. a) Nyquist plots recorded on an LEC device driven at V_{DC} ranging from 2.5 V to 2.8 V (top panel) and 3.1 V to 3.8 V (bottom panel). The solid lines represent the best fit of the equivalent-circuit parameters to the measured data. b) A schematic picture of the LEC device under steady-state operation at $V \geq E_g/e$, with the small open circles representing holes and the small solid circles representing electrons (top), the employed equivalent circuit (middle), and a photograph of the LEC during light emission at V_{DC} = 2.9 V (bottom).

voltage, and that lower values for the EDL thickness can be anticipated at higher applied voltages.

To our understanding this represents the first report on the formation and structure of the EDLs in an LEC device using a combination of impedance spectroscopy and equivalent circuit modeling. The combination of physically sound values for the EDL thickness and the electrode resistances, and the observed good agreement between experimental and model data in Figure 2a provide support for that the employed equivalent circuit is appropriate. In the same context, we wish to mention that the modeling output was found to be rather insensitive to the value for R_{ion}, and that we obtain a good agreement between the model and experiments for values of R_{ion} ranging from 0 to 100 kΩ. We choose to set R_{ion} to 2 kΩ, based on a calculation that considers that the electrolyte constitutes 38% of the active material mass and that a rough estimate for the ambient ionic conductivity of pristine PEO-KCF_3SO_3 is $\sigma = 1 \times 10^{-7}$ S cm^{-1}.[59]

2.3. The Evolving Structure of the Dynamic p–n Junction

When the applied voltage is larger than the bandgap potential of the conjugated polymer ($V_{DC} > E_g/e$), the opportunity for balanced electrochemical doping at the two electrode/active material interfaces has been demonstrated for LEC devices.[1,34,60,61] During this process, a p-type doping region grows from the anodic interface and an n-type doping region grows from the cathodic interface, so that a p–n junction forms in the bulk of the active layer at the position where the two doping fronts meet.[2,28,62] At this p–n junction, subsequently injected electrons and holes recombine to form excitons, which can decay under the emission of light. A schematic view of the operation of an LEC device with a p–n junction in place is presented in the upper part of **Figure 3**b.

Figure 3a presents selected Nyquist plots recorded on ITO/{SY+PEO+KCF_3SO_3}/Al LECs operating under steady-state conditions at applied voltages at or above the bandgap potential of SY ($V_{DC} \geq E_g/e$ = 2.5 V).[28] The Nyquist plots consist of a series of depressed semicircles, with a radius that decreases monotonously with increasing applied voltage. Already at V_{DC} = 2.5 V, light-emission is clearly visible from these devices, thus demonstrating their functionality; a photograph of an LEC device that is emitting significant light (brightness = 290 cd m^{-2}) while driven at V_{DC} = 2.9 V is shown in the bottom part of Figure 3b.

Our proposed equivalent circuit for an LEC device with a fully formed p–n junction (i.e., under steady-state operation at $V_{DC} \geq E_g/e$) is presented in the middle part of Figure 3b. The circuit has been modified in comparison to that of the LEC device driven at V_{DC} = 0 V (see Figure 2b) to consider the formation of doping and a p–n junction structure as well as the fact that the ions are effectively immobile at steady-state, when the ionic diffusion current balances the ionic drift current.[36,63] More specifically, the circuit consists of the same L_{cab} and R_{ext} as in previous cases, but the active layer now comprises two resistors (R_{pdop} and R_{ndop}), which represent the doped regions, and a resistor (R_{pn}) connected in parallel with a CPE element (CPE_{pn}) to take into account the resistive and capacitive components of the intermediately positioned p–n junction. We again find a good agreement between the measured data and the model when a CPE is employed, but note that this agreement turns for the worse if the CPE is replaced by a capacitor (see Supporting Information, Section S2).

From a modeling viewpoint it is difficult to separate R_{pdop} and R_{ndop} from R_{ext}, and we have therefore included their combined value in **Table 3**, where a selection of extracted model data as a function of applied voltage is presented. It is notable that this combined resistance value is essentially identical to R_{ext} for the ion-free OLED device (Table 1) and the undoped LEC device (Table 2) and also independent of the applied voltage, which suggest that R_{pdop} and R_{ndop} are of an insignificant size compared to R_{ext}.

The total resistance for a set of elements, with the same cross-sectional area, connected in series can be calculated using the following equation:

$$R = (1/A) \sum_i \{L_i/(\mu_i n_i e)\} \quad (5)$$

where L_i is the thickness of each element, μ_i and n_i are the average mobility and the concentration, respectively, of the charge carriers in each element, and e is the elementary charge. For the doped regions, we have i = p,n; by using measured and estimated geometric data (A = 0.13 cm^2, $L_p = L_n$ = 35 nm) and estimated values for the mobility ($\mu_p \approx \mu_n = 1 \times 10^{-10}$ m^2 V^{-1} s^{-1})[64] and

Table 3. Selected device data as a function of V_{DC}. R_{ion} was set to 2 kΩ.

V_{DC} [V]	L_{cab} [μH]	$R_{ext} + R_{pdop} + R_{ndop}$ [Ω]	R_{pn} [Ω]	CPE_{pn}		C_{pn} [nF]	d_{pn} [nm]
				Q [$\times 10^{-7}$]	n		
2.5	1.5	30	1300	2.7	0.76	20	23
2.7	1.5	28	280	5.9	0.74	26	18
2.9	1.5	28	93	4.8	0.78	30	15
3.1	1.5	28	43	3.6	0.83	38	12
3.3	1.5	28	25	3.1	0.86	48	10
3.5	1.5	28	17	3.0	0.88	60	7.7
3.7	1.5	28	12	2.9	0.90	77	6.0
3.9	1.5	28	10	3.5	0.89	77	5.9

available literature data for the charge-carrier concentration ($n_p \approx n_n = 2 \times 10^{26}$ m^{-3}), we obtain a value for $R_{pdop} + R_{ndop} \approx$ 2 Ohm, which is much smaller than R_{ext} in agreement with our above observation.

By utilizing Equation (4) with the extracted CPE_{pn} values for Q and n, and setting $R_i = R_{pn}$ (for the parallel resistance in a non-blocking electrode scenario),[56] we find that C_{pn} increases quite markedly with increasing applied voltage up to $V_{DC} = 3.9$ V, after which it begins to decrease. The p–n junction region in LEC devices has been shown to be effectively ion free at steady-state,[36] and a reasonable assumption is thus that its content is a blend of undoped SY and PEO in the same mass proportion as in a pristine device, i.e., 67% SY and 33% PEO. By using the same calculation as for the EDLs in Section 2.2, we obtain a value for the dielectric constant in the p–n junction region of ε_r(pn) = 4.

The values for C_{pn} and ε_r(pn) can be inserted into Equation (1) for the calculation of the effective thickness of the p–n junction region (d_{pn}), and the extracted voltage dependence of d_{pn} and the resistance of the p–n junction region (R_{pn}) are presented in the upper panel in **Figure 4**. In parallel with the impedance measurements, we have also measured the brightness and the current density (j) as a function of applied voltage at steady-state for the same device, and these results are shown in the lower panel in Figure 4.

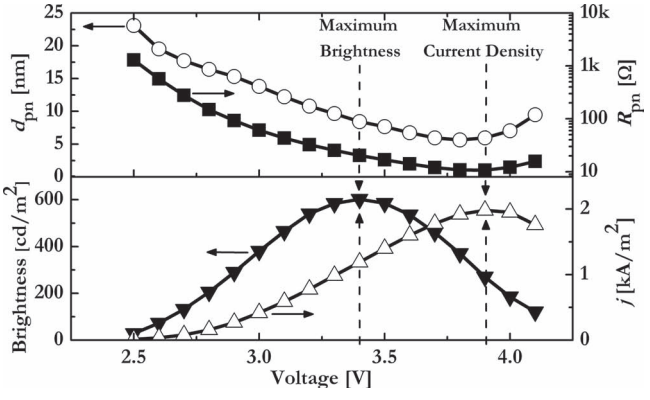

Figure 4. Upper panel: The calculated p–n junction thickness (open circles) and p–n junction resistance (solid squares) as a function applied voltage. Lower panel: The measured brightness (solid downward triangles) and current density (open upward triangles) as a function of applied voltage.

It is interesting that all of the presented data exhibit a strong dependence on the applied voltage, and we call specific attention to that the effective thickness of the p–n junction decreases from $d_{pn} = 23$ nm at $V_{DC} = 2.5$ V to a mere $d_{pn} = 5.2$ nm at $V_{DC} = 3.9$ V. The concept of a thinning p–n junction with increasing voltage is supported by that the resistance of the p–n junction is decreasing in a qualitatively similar manner, and that the current density is observed to increase in a superlinear fashion over a majority of the same voltage range. Beyond $V_{DC} = 3.9$ V the trend is reversed, as d_{pn} and R_{pn} are increasing and j is decreasing, with increasing voltage. It is plausible to attribute this drastic change in behavior to the onset of severe electrochemical[65] and/or chemical[60] side reactions that will limit the current flow and lower the effective conductivity of the p–n junction region (and the doped SY regions).

The measured brightness exhibits a distinctly different behavior, since it reaches its peak value already at $V_{DC} =$ 3.4 V (compare the "maximum brightness" line with maximum "current density" line in Figure 4). This observation can be rationalized by that the light emission is negatively influenced by factors that the conductivity is unaffected by, or even positively influenced by. We propose that the increase in brightness (up to $V_{DC} = 3.4$ V) is attributed to a higher exciton formation rate with increasing current density. At higher applied voltage ($3.4 \text{ V} < V_{DC} < 3.9$ V), the continued increase in the exciton formation rate with increasing current is more than offset by a lowered radiative decay rate of the formed excitons, due to the thinning of the p–n junction. It has been firmly established that the radiative decay rate of excitons in highly doped conjugated-polymer regions in LEC devices is effectively zero, and that a typical diffusion distance for an exciton in a conjugated polymer is ≈10 nm.[66] With this information at hand, it is straightforward to connect the thinning of the p–n junction region to a lowered exciton radiative decay rate, when an increasing and significant fraction of the excitons are diffusing out from the p–n junction into the surrounding doped regions. At $V_{DC} >$ 3.9 V, the brightness will in addition be negatively affected by the onset of various detrimental side reactions.

In this context, we note that Lenes and co-workers used a space-charge-limited approach to obtain information on the

thickness of the p–n junction in LECs based on an ionic transition metal complex.[67] They report that the thickness of the p–n junction continues to decrease during the first 12 h of operation at a set voltage, which interestingly implies that also this device category can operate under the realm of electrochemical doping, but also that the time to reach steady-state can be very long.[67–69]

An important finding of our study is that the steady-state p–n junction structure can depend rather strongly on the applied voltage, as evidenced by the presented evolution of the effective thickness of the p–n junction with changing voltage (Figure 4). As the steady-state structure in LEC devices is attained under conditions of zero net motion of ions (when the ion diffusion flow balances the ion drift flow),[36,64] the absence of a generic doping structure independent on the applied voltage suggests that a full-fledged modeling of LEC devices need to consider also subtle effects, such as the well-established concentration dependence of the mobility for the electronic and ionic charge carriers as well as the electric field dependence of the electronic mobility, in order to be able to pinpoint all details of the complex LEC operation.

3. Conclusions

We have employed a systematic procedure for the extraction of key structural data relevant for the rational design of improved sandwich-cell LECs. We use a combination of impedance spectroscopy and equivalent-circuit modeling to show that thin nanometer-sized EDLs form at low applied voltages and that these ion-based structures assist in electrochemical doping processes at higher applied voltages. When the applied voltage exceeds the bandgap potential of the emitting organic semiconductor, a light-emitting p–n junction structure forms, with an effective thickness that depends strongly on the applied voltage. We show that this adjustment of the p–n junction structure to the applied bias has a profound influence on the device performance of sandwich cell devices, and rationalize the finding of an "ideal" p–n junction thickness of ≈10 nm to a trade-off between an increase in the formation rate and a decrease in the radiative decay rate of the excitons with increasing voltage.

4. Experimental Section

The active material comprised a phenyl-substituted poly(para-phenylene vinylene) co-polymer termed superyellow (SY, PDY-132, Merck) as the CP and the salt KCF_3SO_3 (Sigma Aldrich) dissolved in polyethylene oxide (PEO, Sigma Aldrich, 5×10^6 g mol^{-1}) as the electrolyte. SY, PEO, and KCF_3SO_3 were separately dissolved in cyclohexanone in concentrations of 5 g L^{-1}, 10 g L^{-1}, and 10 g L^{-1}, respectively. After vigorous stirring at 323 K for 48 h, a blend solution was prepared by mixing the SY:PEO:KCF_3SO_3 solutions in a 1:0.5:0.1 ratio. Sandwich cell devices were fabricated by spin-coating carefully cleaned ITO-coated glass substrates (Thin Film Devices) with the blend solution at 2000 rpm for 60 s. The resulting active material film was dried at 343 K for 12 h, before four Al cathodes (thickness = 100 nm, area = 0.13 cm^2) were deposited by thermal evaporation through a shadow mask, so that four identical devices were formed on each substrate.

The devices were driven by, and the current measured with, a Keithley 2400 source-meter. The brightness was measured with a luminance meter (LS-110, Konica-Minolta). The impedance spectra were measured with an Autolab PGSTAT100N potentiostat equipped with an FRA impedance module. A 30 mV AC voltage signal superimposed on a DC voltage (V_{DC}) was used to measure the device impedance as a function of frequency and DC bias. The AC frequency was varied from 1 to 10^6 Hz, and V_{DC} was changed in steps of 0.1 V. Following a change in V_{DC}, the device was allowed to equilibrate for 180 s to allow for the attainment of the steady-state. All measurements were carried out at room temperature in a glove box filled with N_2 ($O_2 < 1$ ppm, $H_2O < 1$ ppm).

Acknowledgements

A.M. acknowledges the support of the Ramon y Cajal programme 08-18-463B-750, Grant MAT2009-14602, Ministerio de Ciencia e Innovación, Spain, and program BEST (Generalitat Valenciana, Spain). The authors acknowledge Kempestiftelserna, Carl Tryggers Stiftelse, and the Swedish Research Council (Vetenskapsrådet) for financial support. L.E. is a "Royal Swedish Academy of Sciences Research Fellow" supported by a grant from the Knut and Alice Wallenberg Foundation.

Received: November 8, 2011
Revised: December 20, 2011
Published online: January 30, 2012

[1] Q. B. Pei, G. Yu, C. Zhang, Y. Yang, A. J. Heeger, *Science* **1995**, *269*, 1086.
[2] G. Yu, Y. Cao, C. Zhang, Y. Li, J. Gao, A. J. Heeger, *Appl. Phys. Lett.* **1998**, *73*, 111.
[3] L. Edman, *Electrochim. Acta* **2005**, *50*, 3878.
[4] J. H. Shin, N. D. Robinson, S. Xiao, L. Edman, *Adv. Funct. Mater.* **2007**, *17*, 1807.
[5] P. Matyba, M. R. Andersson, L. Edman, *Org. Electron.* **2008**, *9*, 699.
[6] S. Tang, K. Irgum, L. Edman, *Org. Electron.* **2010**, *11*, 1079.
[7] J. M. Leger, *Adv. Mater.* **2008**, *20*, 837.
[8] J. Alstrup, M. Jorgensen, A. J. Medford, F. C. Krebs, *ACS Appl. Mater. Interfaces* **2010**, *2*, 2819.
[9] I. V. Kosilkin, M. S. Martens, M. P. Murphy, J. M. Leger, *Chem. Mater.* **2010**, *22*, 4838.
[10] C. V. Hoven, H. P. Wang, M. Elbing, L. Garner, D. Winkelhaus, G. C. Bazan, *Nat. Mater.* **2010**, *9*, 249.
[11] D. A. Pardo, G. E. Jabbour, N. Peyghambarian, *Adv. Mater.* **2000**, *12*, 1249.
[12] Z. B. Yu, X. F. Niu, Z. T. Liu, Q. B. Pei, *Adv. Mater.* **2011**, *23*, 3989.
[13] A. Sandstrom, P. Matyba, O. Inganas, L. Edman, *J. Am. Chem. Soc.* **2010**, *132*, 6646.
[14] K.-H. Yim, Z. Zheng, Z. Liang, R. H. Friend, W. T. S. Huck, J.-S. Kim, *Adv. Funct. Mater.* **2008**, *18*, 1012.
[15] R. Meerheim, R. Nitsche, K. Leo, *Appl. Phys. Lett.* **2008**, *93*, 043310.
[16] Y. Sun, S. R. Forrest, *Appl. Phys. Lett.* **2007**, *91*, 263503.
[17] F. So, J. Kido, P. Burrows, *MRS Bull.* **2008**, *33*, 663.
[18] B. Hirschorn, M. E. Orazem, B. Tribollet, V. Vivier, I. Frateur, M. Musiani, *Electrochim. Acta* **2010**, *55*, 6218.
[19] Z. Chen, X. D. Dang, A. Gutacker, A. Garcia, H. P. Li, Y. H. Xu, L. Ying, T. Q. Nguyen, G. C. Bazan, *J. Am. Chem. Soc.* **2010**, *132*, 12160.
[20] A. Garcia, Y. Jin, J. Z. Brzezinski, T.-Q. Nguyen, *J. Phys. Chem. C* **2010**, *114*, 22309.
[21] Z. B. Yu, L. B. Hu, Z. T. Liu, M. L. Sun, M. L. Wang, G. Gruner, Q. B. Pei, *Appl. Phys. Lett.* **2009**, *95*, 203304.
[22] P. Matyba, H. Yamaguchi, G. Eda, M. Chhowalla, L. Edman, N. D. Robinson, *ACS Nano* **2010**, *4*, 637.
[23] P. Matyba, H. Yamaguchi, M. Chhowalla, N. D. Robinson, L. Edman, *ACS Nano* **2011**, *5*, 574.

[24] G. Mauthner, K. Landfester, A. Kock, H. Bruckl, M. Kast, C. Stepper, E. J. W. List, *Org. Electron.* **2008**, *9*, 164.
[25] C. W. Tang, S. A. VanSlyke, *Appl. Phys. Lett.* **1987**, *51*, 913.
[26] C. D. Muller, A. Falcou, N. Reckefuss, M. Rojahn, V. Wiederhirn, P. Rudati, H. Frohne, O. Nuyken, H. Becker, K. Meerholz, *Nature* **2003**, *421*, 829.
[27] G. G. Malliaras, J. D. Slinker, J. A. DeFranco, M. J. Jaquith, W. R. Silveira, Y. W. Zhong, J. M. Moran-Mirabal, H. G. Craighead, H. D. Abruna, J. A. Marohn, *Nat. Mater.* **2008**, *7*, 168.
[28] P. Matyba, K. Maturova, M. Kemerink, N. D. Robinson, L. Edman, *Nat. Mater.* **2009**, *8*, 672.
[29] Q. Pei, A. J. Heeger, *Nat. Mater.* **2008**, *7*, 167.
[30] Q. B. Pei, Y. Yang, G. Yu, C. Zhang, A. J. Heeger, *J. Am. Chem. Soc.* **1996**, *118*, 3922.
[31] N. D. Robinson, J. H. Shin, M. Berggren, L. Edman, *Phys. Rev. B* **2006**, *74*, 155210.
[32] D. J. Dick, A. J. Heeger, Y. Yang, Q. B. Pei, *Adv. Mater.* **1996**, *8*, 985.
[33] L. S. C. Pingree, D. B. Rodovsky, D. C. Coffey, G. P. Bartholomew, D. S. Ginger, *J. Am. Chem. Soc.* **2007**, *129*, 15903.
[34] L. S. C. Pingree, O. G. Reid, D. S. Ginger, *Adv. Mater.* **2009**, *21*, 19.
[35] J. D. Slinker, J. A. DeFranco, M. J. Jaquith, W. R. Silveira, Y. W. Zhong, J. M. Moran-Mirabal, H. G. Craighead, H. D. Abruna, J. A. Marohn, G. G. Malliaras, *Nat. Mater.* **2007**, *6*, 894.
[36] S. van Reenen, P. Matyba, A. Dzwilewski, R. A. J. Janssen, L. Edman, M. Kemerink, *J. Am. Chem. Soc.* **2010**, *132*, 13776.
[37] Y. Shao, G. C. Bazan, A. J. Heeger, *Adv. Mater.* **2007**, *19*, 365.
[38] Y. Shao, X. Gong, A. J. Heeger, M. Liu, A. K. Y. Jen, *Adv. Mater.* **2009**, *21*, 1972.
[39] J. F. Fang, P. Matyba, L. Edman, *Adv. Funct. Mater.* **2009**, *19*, 2671.
[40] S. Tang, L. Edman, *J. Phys. Chem. Lett.* **2010**, *1*, 2727.
[41] H. J. Bolink, L. Cappelli, E. Coronado, M. Gratzel, E. Orti, R. D. Costa, P. M. Viruela, M. K. Nazeeruddin, *J. Am. Chem. Soc.* **2006**, *128*, 14786.
[42] R. D. Costa, E. Orti, H. J. Bolink, S. Graber, C. E. Housecroft, E. C. Constable, *Adv. Funct. Mater.* **2010**, *20*, 1511.
[43] A. Sandstrom, P. Matyba, L. Edman, *Appl. Phys. Lett.* **2010**, *96*, 053303.
[44] S. Tang, J. Pan, H. Buchholz, L. Edman, *ACS Appl. Mater. Interfaces* **2011**, *3*, 3384.
[45] H. F. Dam, F. C. Krebs, *Sol. Energy Mater. Sol. Cells* **2012**, **97**, 191.
[46] R. Mertens, *The OLED Handbook*, OLED-Info, Herzelia, Israel **2011**.
[47] Y. Li, J. Gao, G. Yu, Y. Cao, A. J. Heeger, *Chem. Phys. Lett.* **1998**, *287*, 83.
[48] T. Ouisse, O. Stephan, M. Armand, J. C. Lepretre, *J. Appl. Phys.* **2002**, *92*, 2795.
[49] C. H. Yang, Q. J. Sun, J. Qiao, Y. F. Li, *J. Phys. Chem. B* **2003**, *107*, 12981.
[50] Z. Yu, M. Wang, G. Lei, J. Liu, L. Li, Q. Pei, *J. Phys. Chem. Lett.* **2011**, *2*, 367.
[51] H. J. Bolink, L. Cappelli, S. Cheylan, E. Coronado, R. D. Costa, N. Lardies, M. K. Nazeeruddin, E. Orti, *J. Mater. Chem.* **2007**, *17*, 5032.
[52] S. van Reenen, P. Matyba, A. Dzwilewski, R. A. J. Janssen, L. Edman, M. Kemerink, *Adv. Funct. Mater.* **2011**, *21*, 1795.
[53] L. Edman, M. A. Summers, S. K. Buratto, A. J. Heeger, *Phys. Rev. B* **2004**, *70*, 115212.
[54] J. C. deMello, N. Tessler, S. C. Graham, R. H. Friend, *Phys. Rev. B* **1998**, *57*, 12951.
[55] J. R. Macdonald, *Impedance Spectroscopy: Emphasizing Solid Materials and Systems*, John Wiley & Sons, New York **1987**.
[56] B. Hirschorn, M. E. Orazem, B. Tribollet, V. Vivier, I. Frateur, M. Musiani, *Electrochim. Acta* **2010**, *55*, 6218.
[57] G. J. Brug, A. L. G. van den Eeden, M. Sluyters-Rehbach, J. H. Sluyters, *J. Electroanal. Chem. Interfacial Electrochem.* **1984**, *176*, 275.
[58] M. B. Armand, P. G. Bruce, M. Forsyth, B. Scrosati, W. Wieczorek, *Energy Materials*, John Wiley & Sons, Ltd, Chichester, UK **2011**, p. 1.
[59] J. R. Dygas, B. Misztal-Faraj, Z. Florjanczyk, F. Krok, M. Marzantowicz, E. Zygadlo-Monikowska, *Solid State Ionics* **2003**, *157*, 249.
[60] T. Wågberg, P. R. Hania, N. D. Robinson, J. H. Shin, P. Matyba, L. Edman, *Adv. Mater.* **2008**, *20*, 1744.
[61] J. Gao, J. Dane, *Appl. Phys. Lett.* **2003**, *83*, 3027.
[62] A. Sandstrom, P. Matyba, L. Edman, *Appl. Phys. Lett.* **2010**, *96*, 053303.
[63] J. C. deMello, *Phys. Rev. B* **2002**, *66*, 235210.
[64] I. Campbell, D. Smith, C. Neef, J. Ferraris, *Appl. Phys. Lett.* **1998**, *72*, 2565.
[65] J. Fang, P. Matyba, N. D. Robinson, L. Edman, *J. Am. Chem. Soc.* **2008**, *130*, 4562.
[66] S. Günes, H. Neugebauer, N. S. Sariciftci, *Chem. Rev.* **2007**, *107*, 1324.
[67] M. Lenes, G. Garcia-Belmonte, D. Tordera, A. Pertegas, J. Bisquert, H. J. Bolink, *Adv. Funct. Mater.* **2011**, *21*, 1581.
[68] H. Rudmann, S. Shimada, M. F. Rubner, *J. Appl. Phys.* **2003**, *94*, 115.
[69] E. S. Handy, A. J. Pal, M. F. Rubner, *J. Am. Chem. Soc.* **1999**, *121*, 3525.